Proceedings of ICRC 2001: 315 © Copernicus Gesellschaft 2001

ICRC 2001

Feasibility study of cosmic ray composition measurements with Cherenkov Telescopes using fractal image parameterization

A. Haungs[1,2] **and J. Knapp**[2]

[1]Institut für Kernphysik, Forschungszentrum Karlsruhe, 76021 Karlsruhe, Germany
[2]Department of Physics and Astronomy, University of Leeds, Leeds LS2 9JT, UK

Abstract. In Earth-bound γ-ray astronomy cosmic rays of 5-500 TeV form the major background. At this energy reliable results on elemental composition of cosmic rays are rare. Direct measurements with balloons or satellites and air shower observations mainly with arrays of particle detectors are stretched to their limits to cover this energy range. An independent measurement of the elemental composition using Cherenkov telescopes promises a better understanding of the composition and provides a test of the simulation programs underlying all the indirect composition estimates. With the air shower simulation program CORSIKA and a detailed simulation of the detector response, Cherenkov images of the Whipple telescope are generated for the cosmic ray (CR) background. The images are parameterized with the well-known Hillas parameterization as well as by fractal and wavelet methods. Special emphasis is given to the recognition of the mass of individual particles.

1 Introduction

Irrespective of ninety years of measurements and the more and more sophisticated experiments and analysis methods the knowledge about the CR elemental composition for primary energies of 10 TeV and above is still poor. The problems are manifold: The low flux of particles limits the statistical accuracy of direct measurements with balloon-borne detectors. Also the estimation and correction of detector efficiencies is increasingly difficult. For indirect measurements via extensive air showers (EASs) the mass resolution is worse due to large intrinsic fluctuations of the showers observables. The conversion of measured observables to primary energy and mass needs indispensably Monte Carlo simulations of the shower development. Here high-energetic hadronic interactions play the key-role in understanding the results. Although for energies close to those in direct measurements accelerator data are available for a calibration of the interaction models, extrapolations to the unknown kinematic region of the extreme forward direction is necessary. Investigations of different observables at the same event or of various independent experiments are necessary to reconstruct the elemental composition and at the same time to understand the interaction mechanisms in more detail.

γ-ray experiments using the atmospheric Cherenkov imaging technique measure as background charged cosmic rays in the interesting energy region of TeV to PeV. The usual method of image parameterization is optimized to separate γ's and hadrons efficiently, irrespective of the masses of the hadrons (Hillas, 1985). Nevertheless there might be a sensitivity of the image parameters to the CR mass. It was shown recently (Haungs et al., 1999), that an alternative parameterization based on fractal and wavelet methods results also in mass sensitive observables. A combination of the parameters may give an alternative measure of the cosmic ray composition in the energy region connecting direct measurements with the results of particle arrays. Additionally, such results would help to advance the understanding of the development of air showers.

Correspondence to: A. Haungs (haungs@ik3.fzk.de)

2 Simulations and image parameterizations

2.1 EAS and telescope simulations

For this analysis sets of simulated images for four CR mass groups were generated. These simulations are performed for the present 10 m-Whipple telescope with a 490 pixel camera (Finley et al., 1999). CORSIKA (v6.0, Heck et al., 1998) is used for the simulation of the shower development and the production of the Cherenkov photons in the atmosphere. High-energy interactions are handled with QGSJET (vers.01, Kalmykov et al., 1997), the low energy part with GHEISHA (Fesefeldt 1985), and the electromagnetic part of the showers is treated by EGS4 (Nelson et al., 1985). 3000 EAS were generated for each primary protons ($E_0 = 0.7 - 200$ TeV), helium nuclei ($E_0 = 0.8 - 300$ TeV), oxygen nuclei ($E_0 =$

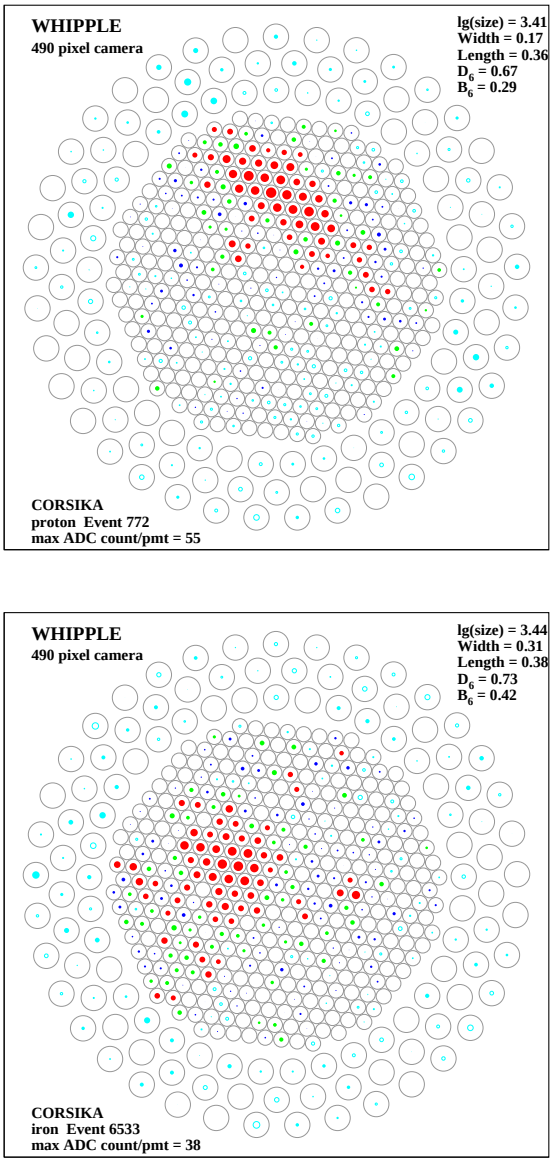

Fig. 1. Examples of simulated Whipple images with the 490 pixel camera. Some of the parameterization results are also given.

$1 - 400$ TeV), and iron nuclei ($E_0 = 2 - 500$ TeV). The energy ranges were chosen that the resulting sizes cover the range of the Whipple measurements. The energy distribution follows a power law with slope -2.7. The showers arrive uniformly from zenith angles of $18.5° - 21.5°$ and azimuth angles of $179.5° - 181.5°$, i.e. covering the field of view of the Whipple telescope pointing to the south with a zenith angle of $20°$. Cherenkov photons reaching the observation level of 2300 m a.s.l. are stored for fifteen virtual Whipple telescopes arranged on a 5×3 rectangular grid with 80/2 m and $80\sqrt{3/4}$ m spacing, such that some of the telescopes form the planned VERITAS configuration. The position of the shower core is scattered from event to event within the telescope array up to 80 m resulting in maximum impact points of up to 180 m. A detailed simulation of the atmosphere, mirror and camera response to the Cherenkov photons is included, as well as a realistic simulation of the night sky background (NSB) (Haungs et al., 2001). For each image the ADC counts of each pixel are stored, and data and simulations are parameterized with the same algorithms. For the parameterization described below, only signals of the smaller inner tubes are taken into account. Fig. 1 shows examples of simulated images from proton and iron showers as seen by the Whipple camera.

2.2 Hillas parameterisation

For the parameterization in terms of first and second order moments only pixels with a signal of $> 4.25\sigma$ of the night sky background (NSB) and neighboring pixels with a signal of $> 2.25\sigma \cdot$ NSB are taken into account. The resulting Hillas parameters can be generally classified into either shape parameters such as *length* and *width* which characterize the extension of the image, or into orientation parameters such as *alpha*, which is the angle of the image length with the direction of the source location within the field of view of the camera. Hadron induced events do not point to a definite source on the sky, hence only the shape parameters can be used. Cherenkov images of showers are mainly elliptical in shape, this is well represented by the *width* and the *length* of the image. Deviations from the ideal elliptical form depending on primary mass might still modify the *width* to *length* ratio.

The *size* of the image is defined as the sum of the ADC counts of those pixels belonging to the image by the definition above. If by chance a pixel exceeds the 4.25σ level, but its position is far away from the image center, it will not change the *size* dramatically, but it will distort the *width* and *length* parameters. On the other hand Cherenkov photons hitting pixels with small entries close to the image center will not be taken into account. The *sum* of the image represents the total content of ADC counts at all inner tubes.

2.3 Fractal and wavelet parameterisation

The development of air showers in the atmosphere varies with primary mass. Different heights of the shower maximum or number of relativistic electrons and muons should be reflected in slightly different distributions and number of Cherenkov photons reaching the telescope. Hence we expect differences in the structure of the images. Pattern recognition tools are for example fractal or wavelet analyses, which result in parameters (multifractal and wavelet dimensions) characterizing the structure of the image of each single event. The idea is to analyse the image on different scale-lengths to reveal deeper structures which may be hidden in a single scale by superimposed Poissonian or Gaussian background fluctuations (Haungs et al., 1999).

For this we divide the image into M = 8, 10, 20, 80, and 320 (with $\nu = log_2\, M$ as fractal scale-length) equally sized, non overlapping cells and calculate the number of ADC counts in each cell. The multifractal moments $G_q(M) = \sum_{j=1}^{M} (k_j/N)^q$

have been computed, with N the total number of ADC counts, k_j the counts in the j^{th} cell and q=2,3,4,5,6 defines the order of the fractal moment. The wavelet moments are $W_q(M) = \sum_{j=1}^{M-1}(\frac{|k_{j+1}-k_j|}{N})^q$, where here the difference of the signals in each scale $(k_{j+1} - k_j)$ defines the moment. G_q and W_q show a proportionality to the length-scale of the form $G_q \propto M^{\tau_q}$ and $W_q \propto M^{\beta_q}$. The exponents lead to the fractal dimensions $D_q = \tau_q/(q-1)$ and wavelet dimensions $B_q = \beta_q/(q-1)$, respectively. Whereas the fractal dimensions characterize more the global structure of the photon distribution in the camera, the wavelet dimensions are more sensitive to local structures.

3 The parameters and their mass sensitivity

Following image parameters are considered for their mass sensitivity: the Hillas parameters *width* and *length*, the fractal parameters D_2 and D_6 and the wavelet dimensions B_2 and B_6. For equal primary energy showers of different masses are expected to have different shapes of the ellipse (*width* to *length* ratio) reflecting the different height of maximum of the shower development in the atmosphere. The fractal dimensions are sensitive to the largest amplitude in the image and how the peak appears on the different length scales. Hence D_2 and D_6 will distinguish between images containing a single large peak in the center and images with several similar sized peaks or smooth distributions. Wavelet parameters examine the differences of neighboring pixels (cells) and how these appear on different length scales. Here light produced by muons or produced at higher altitudes will disperse the image, leading to larger differences from cell to cell and therefore larger wavelet parameters (as example see the right panel in Fig.2).

Heavier primary masses produce less light at observation level for fixed primary energy (Fig.2 left). As the energy is unknown for the recorded images, they have to be classified with the *size* or *sum* of the image. It was found that the mass sensitivity of all the parameters shrinks with *size* or *sum* instead of primary energy (Fig.3). If primary hadrons of different masses produce equal amount of light in the atmosphere, roughly the same shape of the image is expected, but with a flatter and smoother density distribution of the pixels for the heavier primaries (see also Fig. 1). But the *width* increases for heavier primaries due to additional pixels with large amplitudes, presumably from the higher number of muons (Fig.3 left). These additional pixels also change the wavelet parameters (Fig.3 right), but here also smaller amplitudes are taken into account. The fractal parameters, i.e. the overall structure of the image, which are very sensitive parameters for the γ/hadron separation of images (see Haungs et al., 2001) show only poor mass separation for images of same *size*. For both, the fractal and wavelet parameters, the separation improves slightly if they are compared for images of same *sum* instead of *size*. This is understandable, as the *size* does not count the small amplitudes outside the ellipse which influence these parameters.

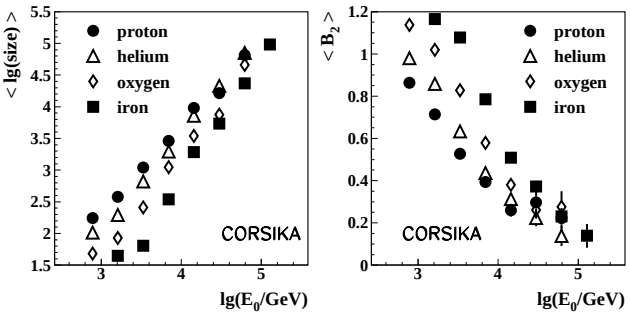

Fig. 2. Mean values of the image parameters *size* and B_2 vs. the primary energy for the different primary particles.

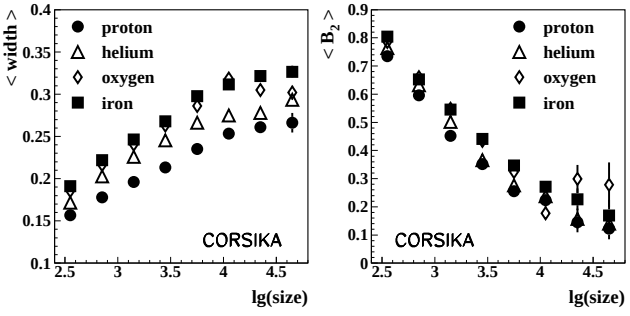

Fig. 3. Mean values of the image parameters *width* and B_2 vs. the *size* of the images for the different primary particles.

The larger the *size*, the better the separation (Fig. 3). This is due to the decreasing event-to-event fluctuation with increasing primary energy (*size* or *sum*). Fig.3 shows the expected mass sensitivity of single parameters. A separation in more than two or three mass groups seems prohibited by the relatively poor mass resolution. Especially for distinguishing between heavier nuclei (e.g. oxygen and iron) the differences at the reconstructed observables are to small. This holds at least for the present Whipple telescope.

4 Neural Net Investigations

We have examined the classification potential of the parameters more quantitatively by an application of an artificial neural net (Lönnblad et al., 1994). The philosophy is that the net is trained with one set and generalized with another independent set of simulated events. The network can then be applied to the measured events, and the events are classified by the network output value. This procedure requires a large set of Monte Carlo generated events, and the number increases about quadratically with the number of input parameters, and with the number of classes. The whole kinematic and geometric range of possibly triggering events have to be covered by simulations. This is fulfilled with the simulations used for this analysis. In a first attempt five input parameters were used and we optimize the net to classify the events in two groups only. For expanding the net to more input parameters or output classes a larger Monte Carlo statistics would be required. We use the inputs: *width*, *length*, D_2, B_2, and

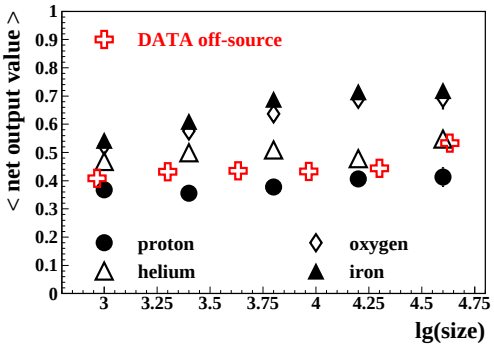

Fig. 4. Average net output values vs. *size* of simulated events for different primary masses and for the measured events.

Table 1. Misclassification matrix: probability that an proton, helium, oxygen, or iron initiated EAS is classified for the light or heavy group. All EAS are taken into account.

	proton	helium	oxygen	iron
light	0.71	0.52	0.36	0.29
heavy	0.29	0.48	0.64	0.71

the *sum*, which are the most independent ones, i.e. with the lowest correlations. In addition to some general cuts (i.e. the Hillas parameterisation was successful and the pixel with the largest ADC count is not at the edge of the inner field of PMTs) we restrict the events to *size* > 500 to be far away from threshold problems for the different primary masses and to cut off most of the images which are produced by single high-energy muons. The net is trained with 2/3 of the simulated proton-sample with output value of zero and 2/3 of the oxygen and iron samples with 1 as output value. After optimizing the net, it is applied to the full Monte Carlo sample and to 3 runs of Crab off-source data. These runs were chosen to have an average zenith angle close to the simulated $20°$ and to be recorded at good seeing conditions. Fig. 4 shows the average net output value dependent on *size* for the different primaries and the real data set. The separation quality increases with increasing *size*. The training of the net does not use helium nuclei, nevertheless applying the net to helium yields values between the proton and the heavy ones. Table 1 lists the classification probabilities of the trained neural net. The two groups light and heavy are separated with a cut in the neural net output value of 0.5.

With help of calculated classification probabilities the fractions of light and heavy induced primaries of a certain *size* range can be deduced by correcting the numbers of misclassified events. Assuming that only proton and iron primaries exist in the data sample, the fraction of the light sample in a *size* range of 4000 to 16000 ADC counts amounts to $\approx 84\%$. With a more realistic assumption that the light group consists of protons and helium nuclei (1.5:1) and the heavy group consists of oxygen and iron nuclei (1:1) the light part increases to $\approx 98\%$. This increase is only due to changes of the classification probabilities used for the correction procedure. For the range of larger *sizes* the light part decrease slightly to $\approx 94\%$.

These results are estimated for ranges of shower *sizes*. Because of the steeply falling primary energy spectrum of the primaries (of all masses) a natural enhancement of the light primaries occurs. A conversion of the results to an elemental composition in terms of primary energy requires a finer binning in ranges of the size and an examination of the energy dependent trigger and reconstruction efficiency of the different masses. This in turn needs a much higher statistics of Monte Carlo events carefully tuned with the observation conditions of the data set to be analysed. Additionally an improvement of the classification probabilities and the number of classification groups should also be possible with increased statistics.

The whole procedure relies on the Monte Carlo model, especially on the modelling of the high-energy hadronic interactions. By comparing results obtained from different models and with results of direct measurements, systematic uncertainties and differences due to these models can be estimated.

5 Summary

In the present study the principal possibility of composition measurements with existing data of imaging Cherenkov telescopes on an event-by-event basis was demonstrated. First applications to data of the Whipple telescope show a large part of light primaries in the energy range of 10 to 100 TeV. This is expected from an extrapolation of the direct measured single mass group spectra. In addition the light induced showers are enhanced by classifying the sample with the shower size, which decreases for fixed energy with the primary mass. A more detailed investigation of the composition with improved statistics is in preparation.

Acknowledgements. A.H. would like to acknowledge the Royal Society of U.K. and the Whipple collaboration for supporting the presented studies at the Leeds University. Special thanks are given to H.Rebel and H.Blümer that they plead for the possibility of these studies within the framework of the Forschungszentrum Karlsruhe.

References

Fesefeldt, H., PITHA-85/02, RWTH Aachen, 1985.
Finley, J.P., et al., AIP Conf.Proc. 515, 301, 1999.
Haungs, A., et al., Astrop.Phys., 12, 145, 1999.
Haungs, A., et al., Proc. of the 27$^{\rm th}$ ICRC, Hamburg, OG 2.4, 2001.
Heck, D., et al., FZKA 6019, Forschungszentrum Karlsruhe, 1998.
Hillas, A.M., Proc. 19$^{\rm th}$ ICRC, La Jolla, Vol.3, 445, 1985.
Kalmykov, N., et al., Nucl. Phys. B (Proc. Suppl.), 52B, 17, 1997.
Lönnblad, L., et al., CERN Preprint, CERN-TH. 7135/94, 1994.
Nelson, W.R., et al., SLAC 265, Stanford Linear Accelerator, 1985.